

Biologically Functional Cationic Phospholipid–Gold Nanoplasmonic Carriers of RNA

Somin Eunice Lee,[†] Darryl Y. Sasaki,[‡] Thomas D. Perroud,[‡] Daniel Yoo,[†] Kamlesh D. Patel,[‡] and Luke P. Lee^{*†}

Biomolecular Nanotechnology Center, Berkeley Sensor & Actuator Center, Department of Bioengineering, University of California–Berkeley, UCSF/UCB Joint Graduate Group in Bioengineering, Berkeley, California 94720-1762, and Sandia National Laboratories, Livermore, California 94551

Received May 28, 2009; E-mail: lplee@berkeley.edu

Abstract: Biologically functional cationic phospholipid–gold nanoplasmonic carriers have been designed to simultaneously exhibit carrier capabilities, demonstrate improved colloidal stability, and show no cytotoxicity under physiological conditions. Cargo, such as RNA, DNA, proteins, or drugs, can be adsorbed onto or incorporated into the cationic phospholipid bilayer membrane. These carriers are able to retain their unique nanoscale optical properties under physiological conditions, making them particularly useful in a wide range of imaging, therapeutic, and gene delivery applications that utilize selective nanoplasmonic properties.

Introduction

Gold nanoparticles (GNPs) in the near-infrared (NIR) spectral region, due to their size and core material, display unique optical properties that make them attractive candidates for drug delivery,^{1–4} gene delivery,^{5–7} biomedical and molecular imaging,^{8–11} and

therapeutics.^{12–20} Because of their large surface area, GNPs are ideal carriers of biomolecules for these applications. While attached to carriers, biomolecules are in an inactive state. When GNP carriers are specifically used to convert light into heat, otherwise known as photothermal conversion,^{21–23} released biomolecules become active to freely interact with the environment. Such optically activated GNP carriers are referred to as nanoplasmonic carriers. In particular, the NIR wavelength regime is well suited for biomedical applications because tissues and cells are essentially transparent at 800–1300 nm.^{24,25} It is possible to obtain very efficient photothermal conversion of energy when the NIR light is matched to the plasmon resonance wavelength of the GNP. Additionally, heat transfer from the surface of GNPs to the surrounding cellular environment is highly localized, decaying exponentially within a few nanometers,^{7,21,26,27} and therefore is thought to have minimal adverse effects on cells. Among the GNPs, rod-shaped GNPs, known as nanorods, are of particular interest due to their large absorption cross-section, a narrow spectral width of the longitudinal plasmon resonance band, and tunability of the

[†] University of California–Berkeley.

[‡] Sandia National Laboratories.

- (1) Sershen, S. R.; Westcott, S. L.; Halas, N. J.; West, J. L. *J. Biomed. Mater. Res.* **2000**, *51*, 293–298.
- (2) Ren, L.; Chow, G. M. *Mater. Sci. Eng.* **2003**, *C23*, 113–116.
- (3) Skirtach, A. G.; Javier, A. M.; Kreft, O.; Kohler, K.; Alberola, A. P.; Mohwald, H.; Parak, W. J.; Sukhorukov, G. B. *Angew. Chem., Int. Ed.* **2006**, *45*, 4612–4617.
- (4) Wijaya, A.; Schaffer, S. B.; Pallares, I. G.; Hamad-Schifferli, K. *ACS Nano* **2009**, *3*, 80–86.
- (5) Chen, C.; Lin, Y.; Wang, C.; Tzeng, H.; Wu, C.; Chen, Y.; Chen, C.; Chen, L.; Wu, Y. *J. Am. Chem. Soc.* **2006**, *128*, 3709–3715.
- (6) Horiguchi, Y.; Niidome, T.; Yamada, S.; Nakashima, N.; Niidome, Y. *Chem. Lett.* **2007**, *36*, 952–953.
- (7) Lee, S. E.; Liu, G. L.; Kim, F.; Lee, L. P. *Nano Lett.* **2009**, *9*, 562–570.
- (8) Copland, J. A.; Eghtedari, M.; Popov, V. L.; Kotov, N.; Mamedova, N.; Motamedi, M.; Oraevsky, A. A. *Mol. Imaging Biol.* **2004**, *6*, 341–349.
- (9) Javier, D. J.; Nitin, N.; Roblyer, D. M.; Richards-Kortum, R. J. *Nanophotonics* **2008**, *2*, 1–12.
- (10) Choi, Y.; Kang, T.; Lee, L. P. *Nano Lett.* **2009**, *9*, 85–90.
- (11) Nallathamby, P. D.; Lee, K. J.; Xu, X. N. *ACS Nano* **2008**, *2*, 1371–1380.
- (12) Huang, X.; El-Sayed, I. H.; Qian, W.; El-Sayed, M. A. *J. Am. Chem. Soc.* **2006**, *128*, 2115–2120.
- (13) Huang, Y. F.; Sefah, K.; Bamrungsap, S.; Chang, H.; Tan, W. *Langmuir* **2008**, *24*, 11860–11865.
- (14) Pissuwan, D.; Valenzuela, S. M.; Killingsworth, M. C.; Xu, X. J. *Nanopart. Res.* **2007**, *9*, 1109–1124.
- (15) Choi, M.; Stanton-Maxey, K. J.; Stanley, J. K.; Levin, C. S.; Bardhan, R.; Akin, D.; Badve, S.; Sturgis, J.; Robinson, J. R.; Bashir, R.; Halas, N. J.; Clare, S. E. *Nano Lett.* **2007**, *7*, 3759–3765.
- (16) Loo, C.; Hirsch, L.; Lee, M.; Chang, E.; West, J.; Halas, N.; Drezek, R. *Opt. Lett.* **2005**, *30*, 1012–1014.
- (17) Skabalak, S. E.; Chen, J.; Au, L.; Lu, X.; Li, X.; Xia, Y. *Adv. Mater.* **2007**, *19*, 3177–3184.

- (18) Gobin, A. M.; O’Neal, D. P.; Watkins, D. M.; Halas, N. J.; Drezek, R. A.; West, J. L. *Laser Surg. Med.* **2005**, *37*, 123–129.
- (19) Hauck, T. S.; Jennings, T. L.; Yatsenko, T.; Kumaradas, J. C.; Chan, W. C. *Adv. Mater.* **2008**, *1–7*.
- (20) Norman, R. S.; Stone, J. W.; Gole, A.; Murphy, C. J.; Sabo-Attwood, T. L. *Nano Lett.* **2008**, *8*, 302–306.
- (21) Cortie, M.; Xu, X.; Chowdhury, H.; Zareie, H.; Smith, G. *Proc. SPIE* **2005**, *5649*, 565–573.
- (22) Khlebtsov, B.; Zharov, V.; Melnikov, A.; Tuchin, V.; Khlebtsov, N. *Nanotechnology* **2006**, *17*, 5167–5179.
- (23) Liu, G. L.; Kim, J.; Lu, Y.; Lee, L. P. *Nat. Methods* **2006**, *5*, 27–32.
- (24) Svoboda, K.; Block, S. M. *Annu. Rev. Biomol. Struct.* **1994**, *23*, 247–285.
- (25) Hirsch, L.; Stafford, R.; Bankson, J.; Sershen, S.; Price, R.; Hazle, J.; Halas, N.; West, J. *Proc. Second Joint EMBS BMES Conf.* **2002**, *1*, 530.
- (26) Skirtach, A.; Dejugnat, C.; Braun, D.; Susa, A.; Rogach, A.; Parak, W.; Mohwald, H.; Sukhorukov, G. *Nano Lett.* **2005**, *5*, 1371–1377.
- (27) Lu, Y.; Liu, G. L.; Kim, J.; Mejia, Y. X.; Lee, L. P. *Nano Lett.* **2005**, *5*, 119–124.

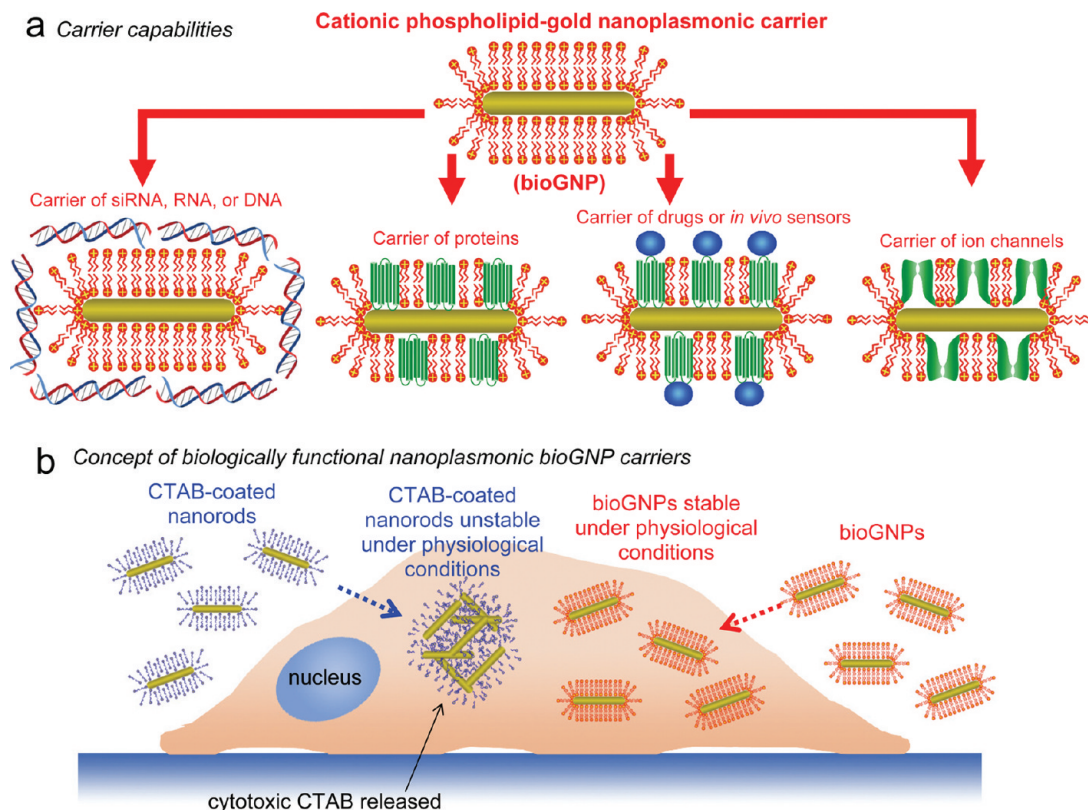


Figure 1. Concept of biologically functional cationic phospholipid–gold nanoplasmonic carriers. (a) The cationic phospholipid bilayer membrane is formed around the gold nanoplasmonic carriers for carrier capabilities. These carriers (bioGNPs) can then be used to carry a variety of biomolecules such as RNA oligonucleotides, DNA oligonucleotides, siRNA, proteins, and drugs by binding to the positively charged surface or by incorporation into the membrane. (b) When CTAB concentration is reduced below the critical micellar concentration, CTAB-coated gold nanorods aggregate under physiological conditions, thereby compromising their unique optical properties. Because CTAB is also known to degrade biomembranes and peptides, CTAB dissociated from the nanorods' surface raises concern regarding cytotoxicity. In contrast, nontoxic bioGNPs are highly stable under physiological conditions, thereby able to retain their unique optical properties for plasmonic-based applications.

longitudinal plasmon resonance wavelength based on aspect ratio. The unique optical properties of gold nanorods arise due to their nanoscale asymmetric geometry and gold core material.

Despite these unique optical properties, the combination of three key factors, carrier functionality, colloidal stability, and cytotoxicity, has hindered the widespread use of gold nanorods as carriers in biological and biomedical applications. Therefore, to harness the full potential of nanomaterials in these applications, the surface coating material as well as the gold core material deserves attention. With respect to cytotoxicity, while the gold core is widely accepted as being biocompatible,¹⁶ bare gold nanoparticles are known to interact with proteins and induce misfolding at physiological conditions.²⁸ Specifically, in the case of gold nanorods, the asymmetric geometry is obtained by synthesizing the nanorods in the presence of a high concentration (>0.1 M) of cetyltrimethylammonium bromide (CTAB), a cationic micellar surfactant that associates preferentially with the {110} crystallographic facet of gold.²⁹ However, CTAB is known to degrade biomembranes and peptides,³⁰ raising significant concern about the cytotoxicity of CTAB-coated nanorods in vitro and in vivo.^{30–35}

The cytotoxic effects of CTAB-coated nanorods can be minimized by reducing the CTAB concentration below the critical micellar concentration,³⁷ but at the expense of the nanorod suspension stability (Figure 1b), consequently compromising their unique optical properties in biological environments. Notably, under physiological conditions, aggregation of nanoparticles has been shown to significantly red-shift and decrease the amplitude of the plasmon resonance band due to closely interacting nanoparticles.^{28,38}

Finally, for plasmon-resonant nanorods to function as biological carriers, biomolecules such as DNA oligonucleotides, RNA oligonucleotides, or small interfering RNA (siRNA) must be able to adsorb on their surface. Notably, in the case of siRNA, chemical modifications may affect the functionality and efficacy

- (28) Zhang, D.; Neumann, O.; Wang, H.; Yuwono, V. M.; Barhoumi, A.; Perham, M.; Hartgerink, J. D.; Wittung-Stafshede, P.; Halas, N. J. *Nano Lett.* **2009**, *9*, 666–671.
- (29) Nikoobakht, B.; El-Sayed, M. A. *Chem. Mater.* **2003**, *15*, 1957–1962.
- (30) Broderick, G.; Craig, M. *J. Dairy Sci.* **1989**, *72*, 2540–2548.
- (31) Cortesi, R.; Esposito, E.; Menegatti, E.; Gambari, R.; Nastruzzi, C. *Int. J. Pharm.* **1996**, *139*, 69–78.

- (32) Ruissen, F.; Le, M.; Carroll, J. M.; vander Walk, P. G. M.; Schalkwijk, J. *J. Invest. Dermatol.* **1998**, *110*, 359–363.
- (33) Huff, T. B.; Hansen, M. N.; Cheng, J.; Wei, A. *Langmuir* **2007**, *23*, 1596–1599.
- (34) Niidome, Y.; Honda, K.; Higashimoto, K.; Kawazumi, H.; Yamada, S.; Nakashima, N.; Sasaki, Y.; Ishida, Y.; Kikuchi, J. *Chem. Commun.* **2007**, *377*, 7–3779.
- (35) Takahashi, H.; Niidome, T.; Kawano, T.; Yamada, S.; Niidome, Y. *J. Nanopart. Res.* **2008**, *10*, 221–228.
- (36) Didychuk, C. L.; Ephrat, P.; Belton, M.; Carson, J. J. L. *Proc. SPIE* **2008**, *6856*, 68560M1–68560M8.
- (37) Connor, E.; Mwamuka, J.; Gole, A.; Murphy, C. J.; Wyatt, M. D. *Small* **2005**, *1*, 325–327.
- (38) Wang, S.; Lu, W.; Tovmachenko, O.; Rai, U.; Yu, H.; Ray, P. C. *Chem. Phys. Lett.* **2008**, *463*, 145–149.

of siRNA.^{39,40} Therefore, the attachment of siRNA onto the surface of gold nanorods without additional chemical modifications to the siRNA themselves is highly desirable. Poly(ethylene glycol) (PEG) has previously been used to modify gold nanorods;^{36,41–43} however, their ability to maximally carry subsequent biomolecules is limited due to the absence of surface charge. Organothiols and polystyrenesulfonate have been used to coat gold nanorods; however, attachment of nucleic acids has not been demonstrated.^{44,45} Synthetic lipids have also been used to modify gold nanorods,^{34,35,46} however, carrier capabilities and/or biocompatibility have not yet been addressed. Polyelectrolyte coating schemes have also been used to coat gold nanorods;^{47,48} however, plasmonic properties under physiological conditions have not yet been discussed. Alternatively, because cationic lipid formulations have already been optimized for both in vitro and in vivo gene transfer over the past decade^{49,50} and many cationic lipid-based gene delivery approaches are currently being tested at the clinical level,^{51,52} validated cationic lipids make ideal candidates for modifying ordinary nanorods into biologically compatible nanorods that simultaneously satisfy carrier functionality, colloidal stability, and noncytotoxicity. The positively charged surface can be used to adsorb negatively charged biomolecules such as RNA oligonucleotides, siRNA, or DNA oligonucleotides (Figure 1b). In addition to carrying siRNA, RNA oligonucleotides, and DNA oligonucleotides, these carriers can also be used to carry a variety of other compounds such as proteins and drugs by incorporation into or binding to the cationic phospholipid membrane (Figure 1a).

In this Article, we present biologically functional cationic phospholipid–gold plasmonic carriers (bioGNPs) that simultaneously exhibit carrier capabilities, demonstrate improved colloidal stability, maintain plasmonic properties, and show no cytotoxicity under physiological conditions. Using an adaptation of vesicle-to-nanoparticle fusion,⁴⁶ we exchanged the cytotoxic CTAB surfactant at the nanorod surface with commercially available cationic phospholipids successfully used for in vivo studies.^{53,54} We first demonstrate that bioGNPs are stable under physiological conditions, thus retaining their unique plasmonic

properties. We then show that the positively charged surface of nanorods can adsorb cargo such as DNA oligonucleotides, RNA oligonucleotides, or siRNA. We finally demonstrate the biocompatibility of bioGNPs via viability/cytotoxicity and cell proliferation studies.

Experimental Procedures

Cell Preparation. The human breast carcinoma lines MCF-7 and BT474 were purchased from the American Type Culture Collection (ATCC). Dulbecco's modified eagle's media (DMEM) was purchased from Invitrogen and was supplemented with 10% heat-inactivated fetal bovine serum, 0.1% nonessential amino acids, and 1% sodium pyruvate. Cells were cultured in the supplemented media and maintained in a 37 °C incubator with 5% CO₂ humidified air.

Synthesis of DNase/RNase-Free Rod-Shaped GNPs. Gold nanorods of aspect ratio 3.0 were synthesized by adapting a previously reported seed-mediated growth method^{29,55} to a DNase/RNase-free environment. Hexadecyltrimethylammonium bromide (CTAB), silver nitrate (AgNO₃), L-ascorbic acid, sodium tetraborate (NaBH₄), and hydrogen tetrachloroaurate (HAuCl₄) were purchased from Alfa Aesar. All solutions were prepared using 0.2 μm filtered nuclease-free water. All glassware and metalware were baked at 240 °C for 24 h to remove exogenous RNase. All pipetting devices and counter space was treated with 70% ethanol. All disposable plastic pipet tips and centrifuge tubes were certified to be free of RNase.

To prepare the seed solution, 5 mL of 0.2 M CTAB solution was mixed with 5 mL of 0.0005 M HAuCl₄. Ice-cold 0.010 M NaBH₄ (0.60 mL) was then added, and the solution was continuously stirred for 2 min at room temperature. To prepare the growth solution, 9.5 mL of 0.1 M CTAB was mixed with 60 μL of 0.10 M AgNO₃, 0.5 mL of 0.01 M HAuCl₄, 55 μL of 0.10 M ascorbic acid, and 12 μL of seed solution with continuous stirring. The gold nanorods were aged overnight at room temperature. After aging 24 h, gold nanorods were separated from the seed solution by centrifugation. At this point, the CTAB concentration in the gold nanorod solution was approximately 0.01 M. The nanorod concentration (approximately 30 μg/mL or 7E11 particles/mL) was confirmed by adjusting to an absorbance of 1 at the longitudinal plasmon resonance wavelength using UV–vis spectroscopy. Aspect ratio was determined by scanning electron microscopy (Hitachi S-4500 FESEM) at 150 000× magnification.

Synthesis of BioGNPs. Commercially available cationic phospholipids Oligofectamine, Lipofectamine 2000, and sc29528 were purchased from Invitrogen and Santa Cruz Biotechnology. Nonionic surfactant Brij56 was purchased from Fluka and prepared in nuclease-free water.

To remove excess CTAB surfactant, 500 μL of unmodified CTAB-coated nanorods (UV–vis absorbance of 1) in 0.1 mM CTAB was centrifuged at 5000 rpm for 10 min. A 10 μL pellet was transferred to a new microcentrifuge tube, redispersed in 500 μL of nuclease-free water such that the final concentration was approximately 0.1 mM, briefly vortexed, and sonicated for 1 min.

To replace CTAB with nonionic Brij56 surfactant at the nanorod surface, nanorods were then centrifuged again at 5000 rpm for 10 min. A 10 μL pellet was transferred to a new microcentrifuge tube, resuspended in 500 μL of 0.01 mM Brij56, briefly vortexed, and sonicated for 1 min.

To replace Brij56 surfactant with a phospholipid bilayer membrane at the nanorod surface, the aforementioned procedure was repeated again to resuspend particles in 50 μL of either Oligofectamine, sc29528, or Lipofectamine 2000. Finally, to remove

(39) Chiu, Y.; Rana, T. *RNA* **2003**, *9*, 1034–1048.

(40) Wang, X.; Nguyen, T.; Gillespie, D.; Jensen, R.; Lu, Z. *Biomaterials* **2008**, *29*, 15–22.

(41) Niidome, T.; Yamagata, M.; Okamoto, Y.; Akiyama, Y.; Takahashi, H.; Kawano, T.; Katayama, Y.; Niidome, Y. *J. Controlled Release* **2006**, *114*, 343–347.

(42) Eghtedari, M.; Liopo, A. V.; Copland, J. A.; Oraevsky, A. A.; Motamedi, M. *Nano Lett.* **2009**, *9*, 287–291.

(43) Liao, H.; Hafner, J. H. *Chem. Mater.* **2005**, *17*, 4636–4641.

(44) Yu, C.; Varghese, L.; Irudayaraj, *Langmuir* **2007**, *23*, 9114–9119.

(45) Leonov, A. P.; Zheng, J.; Clogston, J. D.; Stern, S. T.; Patri, A. K.; Wei, A. *ACS Nano* **2008**, *12*, 2481–2488.

(46) Orendorff, C. J.; Alam, T. M.; Sasaki, D. Y.; Bunker, B. C.; Voigt, J. A. *ACS Nano* **2009**, *3*, 971–983.

(47) Hauck, T. S.; Ghazani, A. A.; Chan, W. C. W. *Small* **2008**, *4*, 153–159.

(48) Gole, A.; Murphy, C. J. *Chem. Mater.* **2005**, *17*, 1325–1330.

(49) Felgner, P. L.; Tsai, Y. J.; Sukhu, L.; Wheeler, C. J.; Manthorpe, M.; Marshall, J.; Cheng, S. H. *Ann. N.Y. Acad. Sci.* **1995**, *772*, 126–139.

(50) Bergan, D.; Galbraith, T.; Sloane, D. L. *Pharm. Res.* **2000**, *17*, 967–973.

(51) Rubin, J.; Galanis, M. E.; Pitot, H. C.; Richardson, R. L.; Burch, P. A.; Charboneau, J. W.; Reading, C. C.; Lewis, B. D.; Stahl, S.; Akporiaye, E. T.; Harris, D. T. *Gene Ther.* **1997**, *4*, 419–425.

(52) Madhusudan, S.; Tamir, A.; Bates, N.; Flanagan, E.; Gore, M. E.; Barton, D. P. J.; Harper, P.; Seckl, M.; Thomas, H.; Lemoine, N. R.; Charnock, M.; Habib, N. A.; Lechler, R.; Nicholls, J.; Pignatelli, M.; Ganesan, T. S. *Clin. Cancer Res.* **2004**, *10*, 2986–2996.

(53) Magin-Lachmann, C.; Kotzamanis, G.; D'Aiuto, L.; Cooke, H.; Huxley, C.; Wagner, E. J. *Gene Med.* **2004**, *6*, 195–209.

(54) Tompkins, S. M.; Lo, C.; Tumpsey, T. M.; Epstein, S. L. *Proc. Natl. Acad. Sci. U.S.A.* **2004**, *101*, 8682–8686.

(55) Gou, L.; Murphy, C. J. *Chem. Mater.* **2005**, *17*, 3668–3672.

excess cationic phospholipids in the solution, bioGNPs were washed twice with nuclease-free water by centrifugation at 5000 rpm for 10 min.

Preparation of BioGNP Carriers. Phosphorothioate 21-mer RNA oligonucleotides conjugated to fluorescein (FAM) dye (488 nm excitation, 532 nm emission) were purchased from Integrated DNA Technologies. The sequence was: 5'GUAGAUUACCACUG-GAGUCUU-FAM-3'. RNase-free 20X Tris-EDTA (TE) buffer was purchased from Invitrogen and was used to prepare 1X TE buffer solution using nuclease-free water.

Stock solutions of RNA oligonucleotides were prepared in RNase-free 1X TE buffer. To 500 μL of bioGNPs, 0.25 μL of 100 μM RNA oligonucleotides was added. The solution was vortexed and allowed to incubate for 1 h. To remove excess oligonucleotides from solution, bioGNPs were washed twice with nuclease-free water by centrifugation at 5000 rpm for 10 min. After preparation of RNA–bioGNP conjugates, an absorbance of 0.2 was measured by UV–vis. By comparing with the original nanorod's UV–vis absorbance of 1, the concentration of bioGNPs was estimated to be approximately 1/5 the original nanorod concentration (approximately 6 $\mu\text{g}/\text{mL}$ or 1.4E11 particles/mL). Because fluorescence quenching by bioGNPs was not observed, bioGNP carriers of fluorescently labeled RNA oligonucleotides were finally visualized using fluorescent microscopy.

Dynamic Light Scattering of BioGNP Carriers. DLS data were collected for all samples using a DynaPro-99-E-15 DLS apparatus from Wyatt Technologies. For each sample, at least 20 scans were performed, each with a 10 s acquisition time, using a scattering angle of 90°. OptiMem medium was purchased from Invitrogen.

CTAB-coated nanorods, Brij56-coated nanorods, and bioGNPs were prepared as described above. DLS measurements were taken of each sample (diluted 1:60 in a quartz cuvette) as-prepared, after washing twice in nuclease-free water, and after resuspending in OptiMem medium.

Internalization Assay of BioGNP Carriers. BioGNP carriers of FAM-labeled RNA oligonucleotides (500 μL) were concentrated into a 5 μL pellet by centrifugation at 5000 rpm for 10 min. MCF-7 cells were harvested and resuspended in DMEM media to a concentration of 240 000 cells/mL. To each well of a 6-well plate, 0.5 mL of cell suspension and 5 μL of concentrated FAM-RNA functionalized bioGNPs were added (120 000 cells/well). The cells were allowed to incubate for 10 h. After 10 h, cells were carefully washed with 1X phosphate buffered solution (PBS), detached using 0.25% trypsin for 2 min, mixed with media 4:1 to deactivate trypsin, collected using centrifugation (1800 rpm, 4 min), and resuspended in 2% paraformaldehyde. Trypan blue was finally added to the cell suspension at 50% concentration to quench uninternalized bioGNP carriers.

As a control, surface receptor ERBB2 on ERBB2-positive BT474 cells was labeled with antibodies conjugated to FITC dye (340553, BD Biosciences). Cells were harvested using 1 mM EDTA for 10 min. Cells were resuspended in surface-staining buffer containing 0.5% bovine serum albumin (BSA) and 0.1% sodium azide in 1X PBS. Five microliters of normal mouse IgG₁ (I8765, Sigma Aldrich) was added, and cells were incubated for 15 min to prevent nonspecific binding of antibodies to Fc receptors. Fifteen microliters of anti-ERBB2-FITC was added, and cells were incubated for 45 min at room temperature. Cells were then washed in surface-staining buffer. Cells were resuspended in 1X PBS containing 2% paraformaldehyde. Trypan blue was finally added to the cell suspension at 50% concentration to quench surface receptors labeled with fluorescent antibodies. LSRII flow cytometer (BD Biosciences) and FlowJo software (Tree Star, Ashland, Oregon) were used to analyze samples.

Visualization of Internalized BioGNP Carriers by Dark-field Light Microscopy. 500 μL of bioGNPs was concentrated into a 5 μL pellet by centrifugation at 5000 rpm for 10 min. Sterile and RNase-free glass coverslips were placed into each well of a 6-well plate. MCF-7 cells were harvested and resuspended in cell culture

media to a concentration of 240 000 cells/mL. To each well, 0.5 mL of cell suspension and 5 μL of concentrated bioGNPs were added on top of the coverslips (120 000 cells/well). The cells were allowed to incubate for 10 h. After 10 h, 2% paraformaldehyde was added to each well to fix cells onto the glass coverslips. For visualization purposes, cell nuclei were stained with DAPI (D1306, Invitrogen) by incubating cells in 300 nM DAPI to each well for 5 min. 1X PBS was then added to each well to wash the cells. A coverslip containing fixed, adhered cells was then placed facedown on a microscope slide, and broadband white light was shined onto the adhered cells from an oblique angle using a darkfield condenser lens. The scattered light alone was collected using a microscope objective lens with a numerical aperture (NA) of 0.65 that was smaller than the NA (1.2–1.4) of the illumination condenser lens.

Viability/Cytotoxicity and Proliferation Analysis. As a standard, liposomes of known concentration and of size similar to that of the commercial phospholipid liposomes were prepared as previously described.⁴⁶ Using these liposomes as standards to compare light intensity measurements, the concentration of the commercial phospholipids was estimated to 6 mM. As a control, unmodified CTAB-coated nanorods were initially resuspended in 6 mM CTAB. Next, 500 μL (30 $\mu\text{g}/\text{mL}$) of bioGNPs or unmodified CTAB-coated nanorods was washed once with nuclease-free water to remove excess lipids/CTAB and was then concentrated into a 5 μL pellet by centrifugation at 5000 rpm for 10 min.

MCF-7 cells were harvested and resuspended in cell culture media to a concentration of 240 000 cells/mL. To each well of a 6-well plate, 0.5 mL of cell suspension and 5 μL of concentrated bioGNPs or unmodified CTAB-coated nanorods were added (120 000 cells/well). The cells were allowed to incubate for 24 h. After 24 h, wells containing cells that were to be analyzed 72 and 120 h later were exchanged with fresh media. Cells that were to be analyzed after 24 h were washed with 1X PBS, detached using 0.25% trypsin for 2 min, mixed with media 4:1 to deactivate trypsin, collected using centrifugation (1800 rpm, 4 min), and resuspended in 0.5 mL of 0.125 μM Calcein AM (Invitrogen). Immediately prior to flow cytometric analysis, 5 μL of PI (BD Pharmingen) was added to stain dead cells for cytotoxicity analysis. Cells are simultaneously analyzed for viability and cytotoxicity using the LSRII flow cytometer within 30 min. This same viability/cytotoxicity staining procedure was repeated after 72 and 120 h of incubation. Cell proliferation was assessed by cell count analysis using a hemocytometer after 120 h of incubation.

Results and Discussion

Gold nanorod carriers were synthesized by modifying a seed-mediated growth approach^{29,55} to be free of DNase/RNase contamination. Using dynamic light scattering (DLS), in Figure 2a and Supporting Information Figure S2, the resultant CTAB-coated nanorod carriers show a size distribution with an average radius of ~ 15 nm (30 nm diameter). Because the nanorod's length was short and the rotational diffusion was therefore rapid, the nanorod was approximated as a translationally diffusing sphere whose diameter equaled the length of the nanorod (30 nm). Lengths based on DLS measurements were in agreement with lengths seen in SEM images (Figure 4a). Because the resultant gold nanorod carriers were coated with CTAB that yielded a net positive surface charge from the quaternary ammonium surfactant headgroup,²⁹ negatively charged, fluorescently conjugated 21-mer RNA oligonucleotides readily attached to the CTAB-coated nanorod carriers, enabling visualization by fluorescent microscopy (Figure 2b). As shown in Supporting Information Figure S4a, while CTAB-coated nanorods were relatively stable and showed a narrow distribution before and after RNA incorporation, an additional population with an average radius of 115 nm appeared in the size

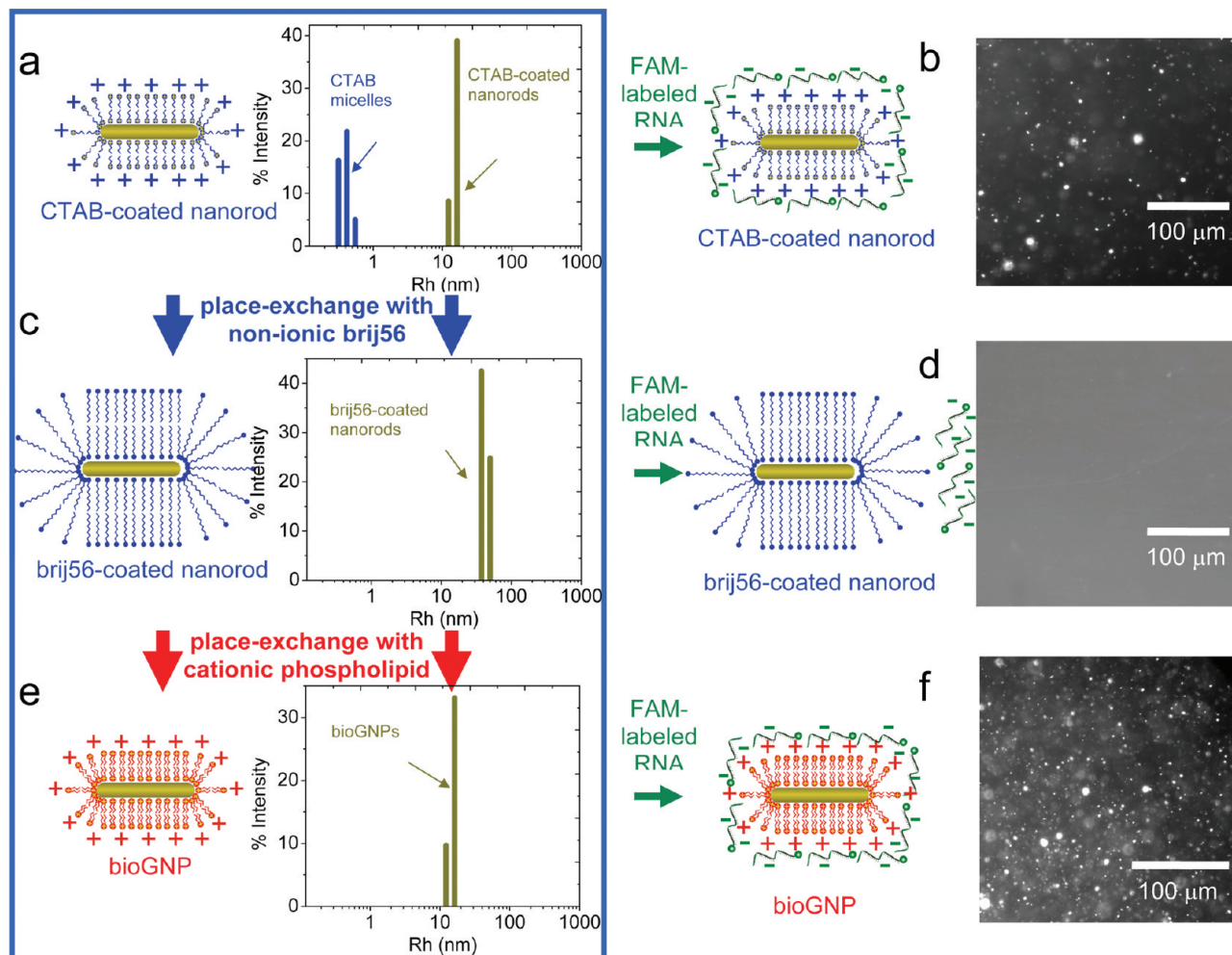


Figure 2. Synthesis of bioGNP carriers. (a) CTAB-coated nanorod carriers are prepared using seed-mediated growth process. Using dynamic light scattering (DLS), CTAB-coated nanorod carriers show a size distribution with an average radius of ~ 15 nm (30 nm diameter). (b) Fluorescent image showing CTAB-coated nanorods carry negatively charged, fluorescent FAM-conjugated 21-mer RNA oligonucleotides. (c) The CTAB surfactant is then place-exchanged with a nonionic surfactant Brij56 surfactant. Using DLS, Brij56-coated nanorods show a size distribution with an average radius ~ 50 nm (100 nm length). (d) Fluorescent image showing that Brij56-coated nanorods are resistant to coupling with fluorescently conjugated RNA oligonucleotides. (e) The Brij56 coating is then place-exchanged with cationic phospholipids to form bioGNPs. Using DLS, bioGNPs show an average radius of ~ 15 nm (30 nm length) with a narrow size distribution. (f) Fluorescent image showing bioGNPs carry negatively charged, fluorescent FAM-conjugated RNA oligonucleotides.

distribution after RNA incorporation, suggesting the possible onset of aggregation of the RNA-CTAB-coated nanorods.

The first stage in demonstrating stable bioGNPs was place-exchanging CTAB with cationic phospholipids vesicles at the nanorod surface by using a vesicle-to-nanorod fusion approach. Excess CTAB surfactant was first removed from the CTAB-coated nanorod solution to yield a final CTAB concentration of approximately 0.1 mM. These CTAB-coated nanorods were then dispersed in various commercially available liposome formulations in approximately 50 fold excess. The phospholipid bilayer coating at the nanorods' surface readily replaced the CTAB surfactant. The formation of phospholipid bilayer coatings on gold nanorods and simultaneous loss of surfactant coatings have been previously determined by NMR and FTIR spectroscopy and zeta potential measurements.⁴⁶

An alternative route to phospholipid-coated nanorods was to first place-exchange the CTAB surfactant with the nonionic surfactant Brij56, followed by place-exchange with cationic phospholipid vesicles. Because CTAB removal from the nano-

rods is essential to minimize cytotoxicity and to eliminate any electrostatic contribution, the latter procedure was developed because it is known that CTAB is capable of inserting itself into lipid bilayers.⁵⁶ Therefore, all of the results henceforth describe the Brij56-to-phospholipid exchange process for coating gold nanorods with a phospholipid bilayer. In Figure 2c, Brij56-coated nanorods show a size distribution with an average radius of ~ 50 nm (100 nm length). The narrow width of the size distribution suggests that Brij56-coated nanorods were stable and with no observed aggregation over a period of weeks. As seen in the fluorescent image of Figure 2d, the Brij56-coated nanorods were resistant to coupling with fluorescently conjugated RNA oligonucleotides. The Brij56 coating was then place-exchanged with various commercially available cationic phospholipids to form bioGNPs by simply exposing surfactant-coated gold nanorods with cationic phospholipid vesicles. BioGNPs show an average radius of ~ 15 nm (30 nm length) with a narrow size distribution (Figure 2e and Supporting Information Figure S1 and S2). The smaller average lengths suggest that the phospholipid bilayer did not layer on top of the Brij56 coating, but instead successfully place-exchanged with the Brij56 at the

(56) Thomas, C. F.; Luisi, P. L. *J. Phys. Chem.* **2005**, *109*, 14544–14550.

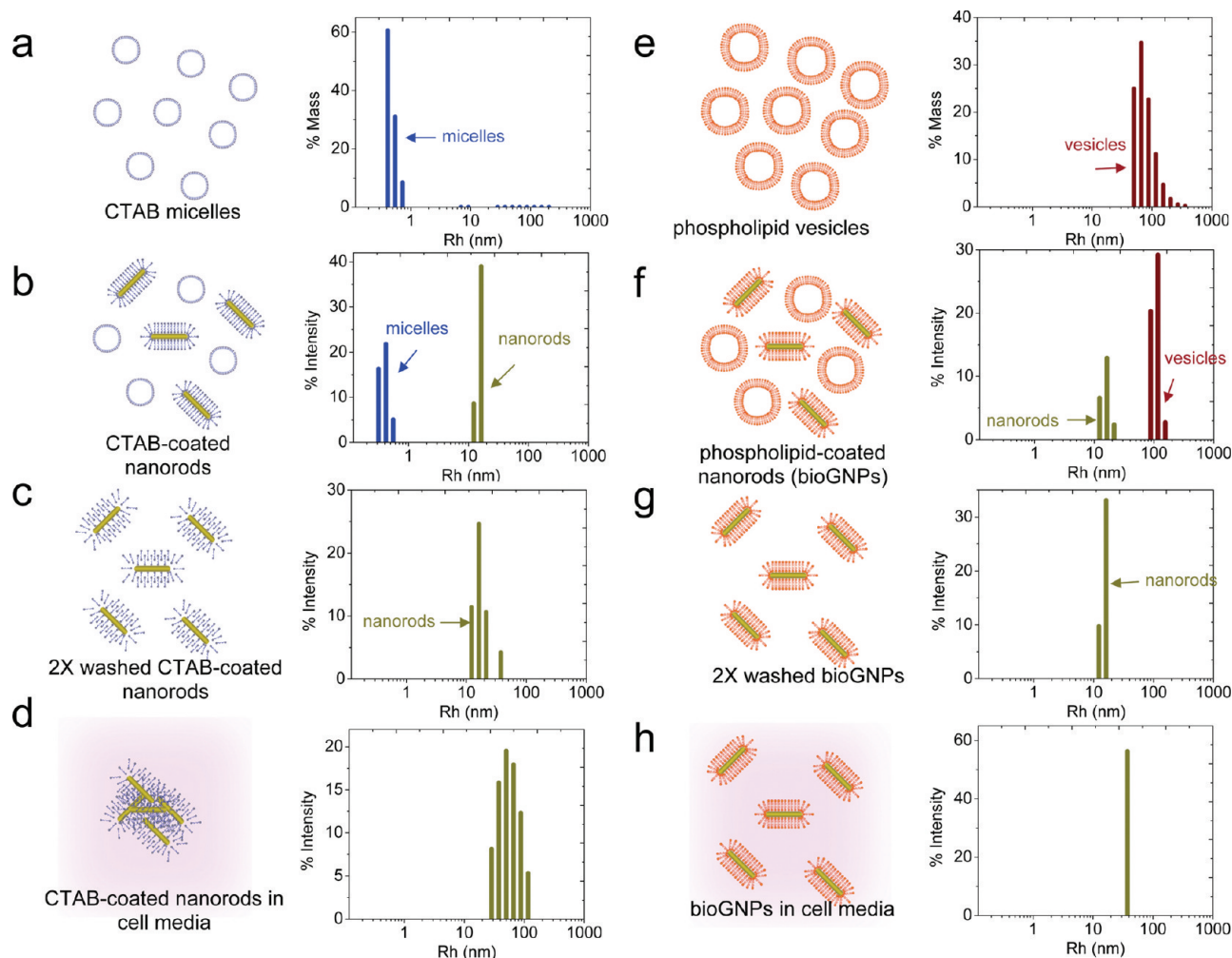


Figure 3. Experimental characterization of bioGNP stability. (a) DLS size distribution of CTAB micelles, (b) DLS size distribution of CTAB-coated nanorods, (c) DLS size distribution of CTAB-coated nanorods that have been washed two times and resuspended in water, (d) DLS size distribution of CTAB-coated nanorods that have been resuspended cell media, (e) DLS size distribution of cationic phospholipid vesicles (sc-29528), (f) DLS size distribution of bioGNPs, (g) DLS size distribution of bioGNPs that have been washed two times and resuspended in water, and (h) DLS size distribution of bioGNPs that have been resuspended in cell media.

bioGNPs' surface. Furthermore, negatively charged, fluorescently conjugated RNA oligonucleotides readily attach to the bioGNP carriers, strongly suggesting that the nonionic surfactant was successfully place-exchanged by a positively charged phospholipid bilayer (Figure 2f and Supporting Information Figure S3). As shown in Supporting Information Figure S4b, bioGNPs showed a narrow distribution before and after RNA incorporation, demonstrating that bioGNP carriers were stable after RNA incorporation. To estimate the amount of RNA attached to bioGNP carriers, fluorescently conjugated RNA oligonucleotides were first attached to bioGNP carriers (approximately 1×10^{11} particles/mL based on UV–vis measurements), and unbound oligonucleotides were subsequently removed from the background solution by centrifugation. Using Triton X-100 detergent to disrupt the cationic phospholipid bilayer around the bioGNP carriers, the bound oligonucleotides were then released from the bioGNP carriers into solution and the fluorescent intensity was measured. To calibrate the fluorescent intensity to the concentration of oligonucleotides, the fluorescent intensities of known concentrations of fluorescently conjugated oligonucleotides were measured (Supporting Information Figure S5). As seen in Supporting Information Figure S5, bioGNPs (approximately 1×10^{11} particles/mL) released

approximately $0.03 \mu\text{M}$ RNA oligonucleotides after treatment with Triton X-100 detergent.

Having established that the CTAB coating can be place-exchanged with a cationic phospholipid membrane, the stability of bioGNPs was then studied and compared against the stability of the CTAB-coated nanorods under biological conditions. CTAB-coated nanorods, which were washed twice and resuspended in nuclease-free water, showed an average radius of ~ 15 nm (30 nm length) with a broad distribution in Figure 3c. The twice-washed CTAB-coated nanorods showed a slightly wider size distribution as compared to as-prepared CTAB-coated nanorods in 0.1 M CTAB solution (Figure 3b), suggesting the onset of aggregation. After resuspending the twice-washed CTAB-coated particles in cell media, further broadening was seen of the size distribution centered at radius of 60 nm, suggesting that particles were highly unstable in cell media (Figure 3d). In comparison, bioGNPs that were washed twice and resuspended in nuclease-free water were highly stable (Figure 2g). When resuspended in cell media, bioGNPs continue to exhibit a narrow size distribution (Figure 2h and Figure S1), thus affirming their excellent stability under biological conditions. Furthermore, optical properties were confirmed using UV–vis spectroscopy. BioGNPs were suspended in water and

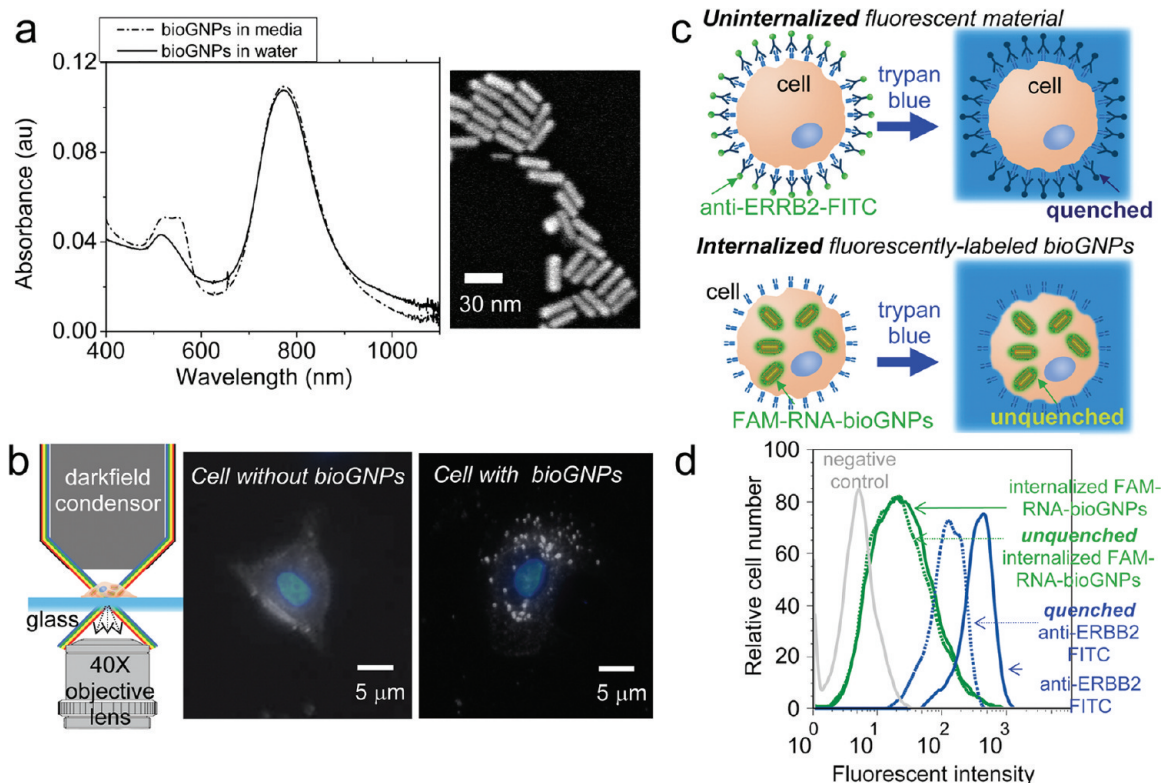


Figure 4. Experimental characterization and internalization of bioGNP carriers. (a) UV–vis absorbance spectra of bioGNPs suspended in water (—), UV–vis absorbance spectra of bioGNPs suspended in media (---), and scanning electron microscopy image of bioGNPs. (b) Schematic of microscope setup, darkfield scattering image of a cell without bioGNPs overlaid with DAPI-stained nuclei image, and darkfield scattering image of a cell containing single bioGNPs overlaid with DAPI-stained nuclei image. (c) Concept of internalization assay where uninternalized fluorescent material (i.e., FITC conjugated ERBB2 antibody) is quenched by trypan blue and internalized fluorescent material (i.e., bioGNP carriers of FAM conjugated RNA oligonucleotides) remains unquenched by trypan blue. (d) Flow cytometric comparison of MCF-7 cells containing unquenched bioGNP carriers of fluorescently labeled RNA oligonucleotides and quenched surface-labeled antibodies (FITC conjugated) recognizing ERBB2 surface receptor on ERBB2-positive BT474 cells. Green solid line represents cells containing bioGNP carriers of fluorescently labeled RNA oligonucleotides in the absence of trypan blue quencher. Green dotted line represents cells containing unquenched bioGNP carriers of fluorescently labeled RNA oligonucleotides in the presence of trypan blue quencher. Blue solid line represents cells that are surface-labeled with fluorescent antibodies in the absence of trypan blue quencher. Blue dotted line represents cells that are quenched surface-labeled with fluorescent antibodies in the presence of trypan blue quencher. Grey solid line represents negative control cells.

were compared to bioGNPs suspended in cell media by UV–vis spectroscopy in Figure 4a. BioGNPs suspended in cell media continue to display a large absorption cross-section and a narrow spectral width of the longitudinal plasmon resonance band, thus confirming bioGNPs' excellent stability under biological conditions.

Having confirmed bioGNPs' stability, we then investigated the internalization of bioGNPs into human cells. Net-positively charged bioGNPs were endocytosed by MCF-7 human breast carcinoma cells by incubation for 10 h. To visualize internalized bioGNPs, the cells were then illuminated with unpolarized white light from an oblique angle using a darkfield condenser lens, and scattered light was collected using a transmission-mode darkfield microscope (Figure 4b). To locate cells' nuclei, darkfield scattering images were overlaid with DAPI-stained images. It is clearly evident from Figure 4b that scattered light from cells containing bioGNPs is easily differentiated from that from cells lacking bioGNPs.

To further confirm that bioGNPs were in fact internalized within cells and not externally adsorbed onto the cells' surface, MCF-7 cells were first exposed for 10 h to bioGNP carriers of fluorescently labeled RNA oligonucleotides. Uninternalized carriers were then rendered nonfluorescent by using trypan blue as a quencher. Because trypan blue absorbs light between 475

and 675 nm,^{57,58} the emission of fluorescent dyes within this wavelength range is quenched in the presence of trypan blue. If bioGNP carriers of FAM-labeled RNA oligonucleotides (excitation 495 nm, emission 520 nm) are indeed internalized within cells, it is expected that their fluorescence should remain unquenched when cells are resuspended in trypan blue. Flow cytometry results displayed in Figure 4 confirm that the majority of the bioGNP carriers of FAM-labeled RNA oligonucleotides remained fluorescent within the protective confines of intact cell membranes. In contrast, as a control, surface receptor ERBB2 (also known as HER-2, neu, and EGFR-2) on ERBB2-positive BT474 breast carcinoma cells were labeled with antibodies conjugated to FITC dye (excitation 488 nm, emission 532 nm). To inhibit internalization by receptor-mediated endocytosis, FITC-conjugated antibodies were bound in the presence of sodium azide. Flow cytometry results in Figure 4 show that surface-bound FITC on control cells was efficiently quenched in the presence of trypan blue (Figure 4d).

Finally, the biocompatibility of bioGNPs was investigated and compared against unmodified CTAB-coated nanorods by conducting a long-term viability/cytotoxicity and proliferation

(57) Wang, R.; Kovalchin, J. T.; Muhelnkamp, P.; Chandawarkar, R. Y. *Blood* **2006**, *107*, 1636–1642.

(58) Perroud, T. D.; Kaiser, J. N.; Sy, J. C.; Lane, T. W.; Branda, C. S.; Singh, A. K.; Patel, K. D. *Anal. Chem.* **2008**, *80*, 6365–6372.

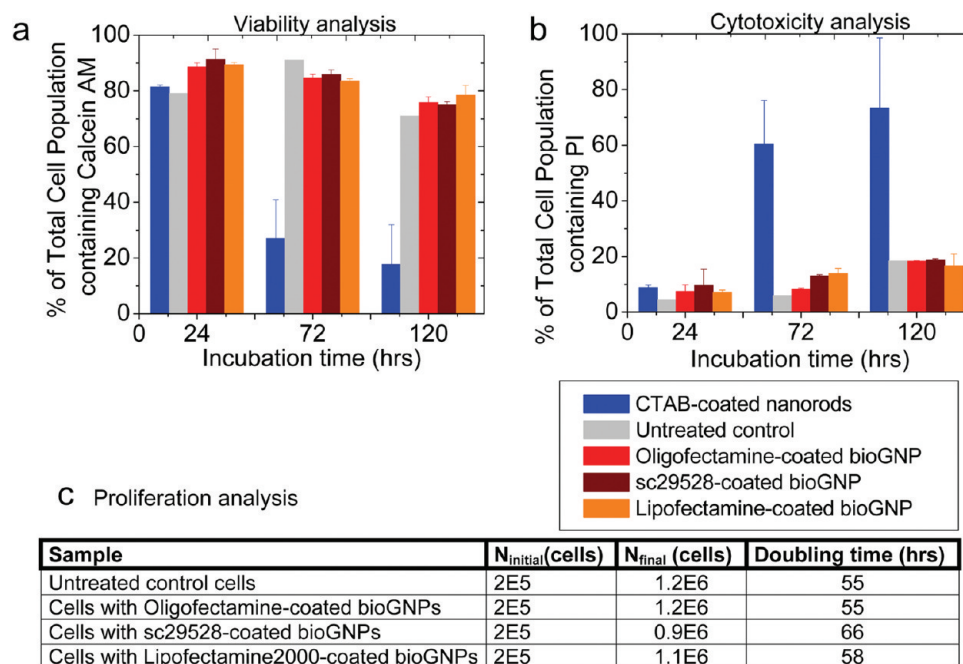


Figure 5. Biocompatibility analysis of bioGNPs. (a) Viability analysis – flow cytometric results of viability using Calcein AM after 24, 72, and 120 h incubation with nothing, CTAB-coated nanorods, Oligofectamine-coated bioGNPs, sc29528-coated bioGNPs, and Lipofectamine2000-coated bioGNPs; (b) cytotoxicity analysis – flow cytometric results of cytotoxicity using PI after 24, 72, and 120 h incubation with nothing, CTAB-coated nanorods, Oligofectamine-coated bioGNPs, sc29528-coated bioGNPs, and Lipofectamine2000-coated bioGNPs; and (c) proliferation analysis – table summarizing initial cell count (N_{initial}), final cell count after 120 h (N_{final}), and calculated doubling times for cells containing nothing, Oligofectamine-coated bioGNPs, sc29528-coated bioGNPs, and Lipofectamine2000-coated bioGNPs.

studies in MCF-7 cells. Viability/cytotoxicity was conducted using a two-color fluorescence assay to simultaneously determine numbers of live and dead cells. Calcein AM, a dye that converts from nonfluorescent cell-permeant calcein AM into fluorescent cell-impermeant calcein by intracellular esterase enzymes in living cells, was used as a measure of cell viability. Propidium iodide (PI), a dye that enters through permeabilized membranes of compromised cells, was used as a measure of cell cytotoxicity. The concentration of commercial cationic phospholipids was estimated to be approximately 6 mM based on DLS comparison with standards of known concentration. Unmodified CTAB-coated nanorods were therefore initially resuspended in 6 mM CTAB to obtain comparable results. Unmodified CTAB-coated nanorods and bioGNPs were then washed with nuclease-free water to remove excess lipids/CTAB and resuspended in cell media. Based on DLS measurements, bioGNPs were highly stable while unmodified CTAB-coated nanorods were only moderately stable in cell media. To retain unique optical properties of stable nanoparticles, further washing was avoided because twice-washed CTAB-coated nanorods tend to strongly aggregate in cell media as seen in DLS measurements in Figure 3d. After 72 and 120 h of incubation, based on flow cytometric data, viability (Figure 5a) and cytotoxicity (Figure 5b) of cells containing bioGNPs were statistically significant from cells containing unmodified CTAB-coated nanorods (also see Supporting Information Figure S6). It is apparent that cells containing bioGNPs are viable, whereas cells containing CTAB-coated nanorods are compromised. Clearly, bioGNP carriers are a superior alternative to unmodified CTAB-coated nanorods for biological studies.

Cell proliferation was also assessed by cell count analysis after 120 h of incubation with and without bioGNPs. Based on cell count analysis, doubling times were then determined for

bioGNP-containing samples and compared to an untreated control sample. Doubling time of 55 h for the untreated control sample was in agreement with doubling times previously reported in literature for MCF-7 cells.⁵⁹ Cells containing bioGNPs exhibited doubling times approximately similar to that of the untreated control sample (Figure 5c), verifying that incubation with bioGNPs did not adversely affect proliferation of MCF-7 cells.

While in vitro experiments were successfully demonstrated here, we anticipate developing bioGNP carriers for use in vivo mammalian and nonmammalian model systems. BioGNP carriers can be coated with cationic phospholipid formulations specifically optimized for biodistribution in vivo. In addition to carrying siRNA, RNA oligonucleotides, and DNA oligonucleotides for gene delivery applications, bioGNPs can also be used to carry a variety of other compounds such as proteins and drugs for in vivo applications.

Conclusions

In closing, we have designed biologically functional phospholipid–gold plasmonic bioGNP carriers that exhibit carrier capabilities, demonstrate improved nanoparticle stability, and show no cytotoxicity under physiological conditions. Successful demonstration of these advantages has been shown here using mammalian cell lines. In addition to these advantages, because bioGNPs are able to retain their unique optical properties under physiological conditions, we anticipate that bioGNPs will be particularly useful in a wide range of applications that utilize selective nanoplasmonic properties. We therefore expect bioGNPs to have important implications in

(59) Barnes, J. A.; Dix, D. J.; Collins, B. W.; Luft, C.; Allen, J. W. *Cell Stress Chaperones* **2001**, *6*, 316–325.

advancing drug delivery, gene delivery, biomedical and molecular imaging, and therapeutics.

Acknowledgment. We acknowledge the National Physical Science Consortium (NPSC) graduate fellowship for support of S.E.L. We thank Terry Johnson and Dave Robinson for technical insight. We thank the UC Berkeley undergraduate students Dana Donnenwirth, Daniel Rosen, Gabe Sudario, and Alan Wilk for assistance with viability/cytotoxicity experiments. We also thank Ann Fischer and Michelle Yasukawa of the UC Berkeley Tissue Culture Facility for long-term maintenance of MCF-7 and BT474 cell lines. We acknowledge the Division of Materials Science and Engineering in the Department of Energy Office of Basic Energy

Sciences for financial support of D.Y.S. at Sandia. Sandia is a multiprogram laboratory operated by Sandia Corp., a Lockheed Martin Co., for the United States Department of Energy under Contract DE-AC04-94AL85000.

Supporting Information Available: Supporting DLS measurements, additional fluorescent images after FAM-RNA incorporation onto bioGNPs, experimental estimation of amount of RNA on bioGNPs, and additional flow cytometric data. This material is available free of charge via the Internet at <http://pubs.acs.org>.

JA904326J